Impact-induced solidlike behavior and elasticity in concentrated colloidal suspensions

Baojin Chu and David R. Salem

Phys. Rev. E **96**, 042601 — Published 5 October 2017

DOI: 10.1103/PhysRevE.96.042601

Impact induced solidlike behavior and elasticity in concentrated colloidal suspensions

Baojin Chu,[1,*] and David R. Salem[2,*]

[1]*Department of Materials Science and Engineering, CAS Key Laboratory of Materials for Energy Conversion, University of Science and Technology of China, Hefei, Anhui Province, China 230026*

[2]*Composites and Polymer Engineering (CAPE) Laboratory, South Dakota School of Mines and Technology, Rapid City, South Dakota 57701*

PACS number(s): 83.80.Hj, 83.60.Rs, 83.90.+s, 47.57.-s

Abstract

Modified drop weight impact tests were performed on SiO_2/ethylene glycol concentrated suspensions. Counterintuitive impact-induced solidlike behavior and elasticity, causing significant deceleration and rebound of the impactor, were observed. We provide evidence that the observed large deceleration force on the impactor mainly originates from the hydrodynamic force, and that the elasticity arises from the short-range repulsive force of a solvation layer on the particle surface. This study presents key experimental results to help understand the mechanisms underlying various stress-induced solidification phenomena.

* chubj@ustc.edu.cn

* david.salem@sdsmt.edu

I. INTRODUCTION

Concentrated particulate suspensions consisting of liquids and particles with nanometer or micrometer diameter have been extensively studied because of their interesting rheological behaviors [1-6]. Although these suspensions are initially fluid, some can exhibit behaviors more akin to solids under an external load. For example, when a shear stress is applied to these suspensions, shear thickening (an increase in the viscosity with an applied shear rate or stress) can be observed above a critical shear rate or stress [2]. In some extreme cases, after applying shear stress, part of the energy can be stored in the suspensions, causing a reverse rotation of the plate used for the rheological measurements, indicating the elasticity of the suspensions [3]. Some concentrated suspensions can also exhibit solidlike behavior under normal stress. One intriguing example is that a person can run on a concentrated cornstarch/water suspension as if it were a solid surface. There are also other observations of solidlike behavior in concentrated suspensions under dynamic tensile and compressive loads. Concentrated poly(methyl methacrylate) spheres/octadecene suspensions have been shown to fracture like solids, and the suspension filament elastically recoils under extension when it breaks [4]. Focused force transmission has been observed when a concentrated cornstarch/water suspension was impacted by a solid sphere [5], and the impact of a projectile can create cracks in concentrated cornstarch/water suspensions, like brittle solid materials [6].

The mechanisms of this counterintuitive stress-induced solidlike behavior in concentrated suspensions are still not fully understood. For shear thickening, several

models, including order-disorder transition, hydroclusters, or dilatancy and jamming, have been proposed [2,4,7-14]. These models have been successfully applied to some suspensions, but a general microscopic model is still lacking [13,14]. To explain the impact-induced solidlike behavior in cornstarch/water suspensions, a snowplow model with unlimited growth of a solid region under impact was proposed [15]. However, concentrated cornstarch/water suspensions frequently exhibit shear thickening behavior, and the potential involvement of shear thickening in the underlying mechanisms of the impact-induced solidlike behavior in shear thickening suspensions remains an important, unresolved area of inquiry. Furthermore, the snowplow model attributes the large deceleration force to the viscous force of the growing solid front, but the microscopic mechanisms of the viscous force are not explained.

In addition to its fundamental scientific importance, understanding stress-induced solidlike behavior is indispensable for some important applications of concentrated suspensions, such as designing new lightweight body armor and energy absorbent devices [16,17]. Studies have shown that shear thickening fluids can enhance the energy absorption of polymeric fabrics, and this phenomenon has been exploited to improve the ballistic impact or stab resistance of fabrics, or attenuate the impact force transmitted through the suspensions [16-18]. Again, the microscopic level mechanisms for energy dissipation and force attenuation are not clear.

In this work, to understand the stress-induced solidlike behavior in concentrated suspensions, modified drop weight impact tests were performed on dense silica/

ethylene glycol (EG) suspensions. A similar impact study has been performed on cornstarch/water suspensions by Waitukaitis and Jaeger, as mentioned earlier [15]. In addition to using different equipment and suspensions, our study differs from their work in the following aspects: First, in Waitukaitis and Jaeger's study, the authors focused their analysis on the observed large deceleration force on the impactor. In this study, we attempt to examine the relationship between the impact induced solidlike behavior and the shear thickening behavior of the dense suspensions by closely analyzing the correlations among the experimental data of the force, velocity and displacement. In so doing, we provide strong evidence that the impact-induced solidlike behavior and shear thickening are correlated. Second, we intentionally performed the impact tests on dense suspensions with a small sample size. In this way we were able to induce stronger solidlike behavior and to analyze the governing force for the observed solidlike behavior. Evidence suggests that the observed large impact force and significant energy dissipation, which are associated with the stress-induced solidlike behavior, appear to originate from the interparticle hydrodynamic lubrication force. Furthermore, elasticity, which is manifested by a significant rebound of the impactor, was observed in the suspensions exhibiting a strong impact-induced solidlike behavior. It is proposed that the stress induced elasticity may arise from a repulsive force from the solvation layer on the surface of the particles. The mechanisms of the impact-induced solidlike behavior are also discussed, which may shed light on a general model for the interpretation of stress-induced solid-like behavior in concentrated suspensions.

II. METHODS

Silica (SiO_2) particles (particle size of approximately 550 nm, density of approximately 1.8 g cm^{-3} and polydispersity <10%) were purchased from Fiber Optic Center, Inc (New Bedford, MA, USA). Dense silica/ethylene glycol (EG, from Sigma Aldrich, viscosity of 1.61×10^{-2} Pa.s and density of 1.113 g cm^{-3}) suspensions with concentrations above 65 wt % were mixed (in SpeedMixer, DAC 600) at a speed of 1500 rpm for 20 minutes. The viscosity of the suspensions under various shear rates and stresses was tested using a TA Instruments ARES G2 rheometer in a plate-plate geometery (plate diameter of 25 mm) at room temperature. The gap between the two plates was 1 mm. A logarithm flow-sweep protocol was selected with 10-20 measurement points per decade to obtain reproducible rheograms. Additional details of the rheometry protocol are given in ref. [19]. Instrumented drop weight impact tests are often performed on composite materials to study the low velocity impact response of the materials, and hemispherical impactors are frequently used in those studies [20]. In our study, a circular plate impactor was used to study the solidlike behavior of the concentrated suspensions under impact. The impact tests of the suspensions were performed on a Ceast 9350 Drop Weight Impact Testing System. The suspensions were contained in a transparent polypropylene plastic cup (diameter of 3.5 in, wall thickness of ~1.6 mm) and were impacted using a custom-made titanium flat surface impactor (diameter 2.5 inch). The total mass of the impactor was 5.205 kg. The impact speed varied from 0.5 m s^{-1} to 4 m s^{-1}, and these speeds correspond to impact energies of approximately 0.63 J to approximately 40 J. The depth of the silica/EG

suspensions ranged from approximately 28 mm to 40 mm. After each test, the suspensions were remixed to homogenize them. The impact process was simultaneously recorded using a high-speed camera (Motionpro). A transparent container was used to facilitate the observation of behavior of the fluid under impact. The deceleration force experienced by the impactor was recorded by a force sensor embedded in the impactor. The velocity and displacement of the impactor were automatically obtained by the equipment software via integration based on the measured force and the calculated acceleration. The specifications of the force sensor (load cell) used in our study are as follows: the maximum capacity is 10 kN; the linearity and the repeatability of the data are < ±0.25% and < 0.25% of reading over a range of 1% to 100% of load cell static rating, respectively; the zero balance (the signal of the load cell in the no load condition) is < ±10% of rated output up to 100 N and < ±5% of rated output for 500 N and above. These specifications indicate that the zero-balance value cannot be considered an absolute value for loads below 500N, since it may be in error by as much as ± 100N, but that the force values relative to the set zero value will be repeatable to < ±0.25%. Due to the capability of the load cell, the data may deviate significantly from their absolute values in the small force range (<500N), but their relative changes should be accurate. Therefore, for small forces measured in this study, especially the data from the suspensions of lower concentrations, they are deemed relative values, but not absolute ones.

III. RESULTS AND DISCUSSION

A. Correlation between the impact-induced solidification and shear thickening

Figure 1(a) shows the viscosity of the suspensions at different concentrations under shear stress. At silica concentrations above 65 wt % (53.4 vol %), all the suspensions exhibit shear thinning when the shear rate is low, followed by shear thickening above a critical shear rate. As the concentration of particles increases, the behavior becomes stronger, and the critical shear rate shifts to a lower value. The two-stage (shear thinning/shear thickening) rheological behavior of the silica/EG suspensions is consistent with other studies [2,11,17], and can be of great advantage for some practical applications. For example, for armor applications, the fluid can provide low resistance to moderate rates of deformation for standard usage (the shear thinning regime), such as the abrupt movements of a person wearing the fluid impregnated body armor, but high resistance under severe deformation rates (the shear thickening regime), such as those associated with the penetration of lethal projectiles. Figure 1(b) shows the morphology of the silica particles used in this study, which are spherical with a diameter of approximately 550 nm.

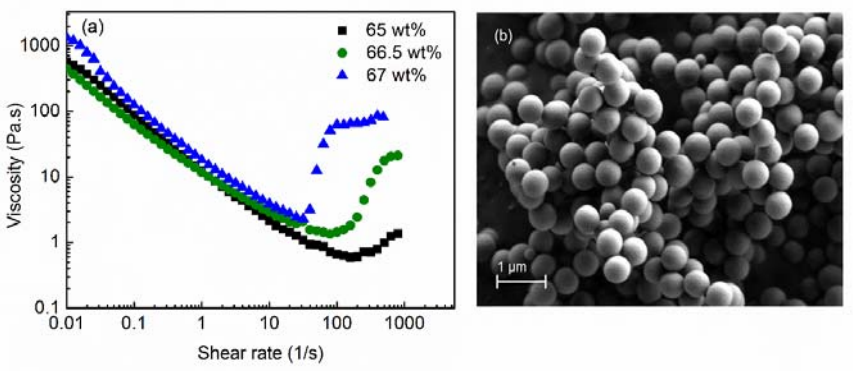

FIG. 1. (a) Viscosity vs. shear rate curves for the silica particle/ethylene glycol colloidal suspensions; (b) SEM image of the silica particles.

The impact test was first performed on a suspension with 65.5 wt % (54.0 vol %) SiO_2. According to Fig. 1(a), the suspension exhibits a weak shear thickening, which can also be felt when stirred by hand. Movie 1 in the Supplemental Material shows the behavior of the suspension under an initial impact speed of 1.07 m s^{-1} [21]. As shown in the movie, the entry of the impactor into the suspension causes a large splash of fluid, a phenomenon that is often seen in regular fluids [22,23]. The time dependence of the deceleration force on the impactor, deformation (or displacement), and velocity of the impactor during the impact test was presented in Fig. 2. From the deceleration force vs. time curves of the impact tests under various initial impact speeds, which were summarized in in Fig. 3(a), we can see two force peaks on each curve. The second peaks on these curves have a much higher magnitude and occupy a broader time range than the first peaks, leading to much more significant deceleration of the impactor (and also energy dissipation), as shown in Fig. 2. The first force peak, according to prior studies on impact tests with regular fluids, is related to the momentum transfer from the impactor to the fluid [22,23], causing the splashing seen

in the impact test video (supplementary material, movie 1). The first peak appears in impact studies on normal fluids and is not specific to our study, but the second peak is unusual in normal fluids. Similar second peaks have been attributed to solidification in ref. [15]. Our results indicate that the 65.5 wt % suspension was originally fluid after the impact was initiated, and transformed into a solidlike state in the final stage of the impact, resulting in the significant deceleration of the impactor.

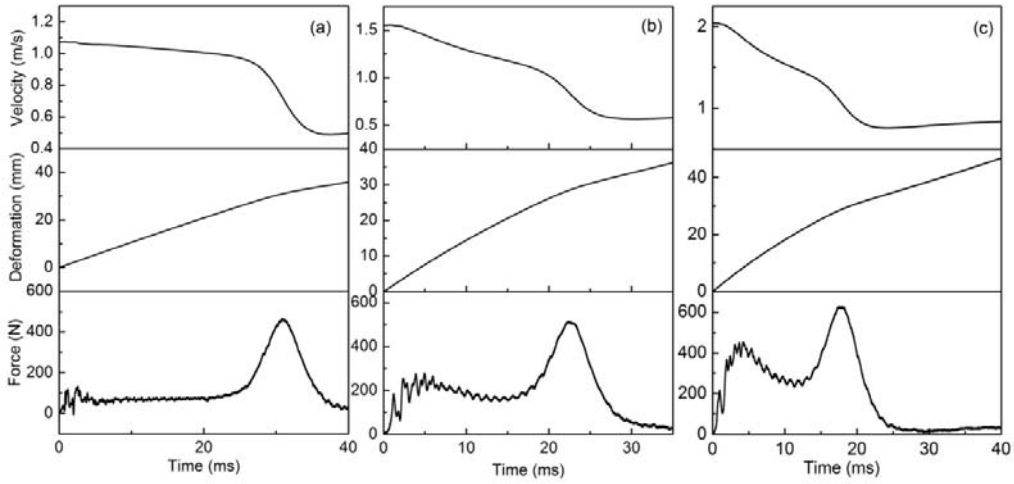

FIG. 2. Deceleration force, deformation of the suspension (or displacement of the impactor), and impactor velocity vs. time for the 65.5 wt % silica suspension under initial impact speeds of (a) 1.07 m s^{-1}, (b) 1.55 m s^{-1}, and (c) 2.03 m s^{-1}.

In addition to shear flow, viscous materials are often tested by squeezing flow. This test is performed by squeezing materials between two parallel plates under controlled conditions, such as controlled volume, area or speed [24-26]. Our impact test of the suspensions was similar to the so-called imperfect squeezing flow test as a result of using a flat surface plate and a container with a flat bottom; but is unlike the normal squeezing test because the impact test is a dynamic test in which the speed of the impactor varies continuously with time [26]. Considering that all the tests were

carried out on a similar time scale, the results obtained by varying impact speeds should still be comparable. The normal force F under constant area squeezing flow with perfect slip between the plates and the viscous fluid can be expressed as [24,25]:

$$F = 3\mu(\dot{\gamma})\dot{x}(t)A_0, \tag{1}$$

where μ is the shear viscosity, $\dot{\gamma}$ is the shear rate in the shear flow, $\dot{\gamma} = \sqrt{3}\dot{x}(t)$, and A_0 is the area of the impactor. The squeezing strain rate $\dot{x}(t)$ is defined as

$$\dot{x}(t) = v(t)/x(t), \tag{2}$$

where $v(t)$ is the speed of the impactor, $x(t) = l_0 - D(t)$ is the distance from the bottom of the container, l_0 is the original depth of the suspension, and $D(t)$ is the displacement of the impactor. In our study, both the impactor and plastic container have very smooth surfaces, and it is reasonable to assume that the requirement of perfect slip between the suspension and the plate is met. Using the results shown in Fig. 2, the curves of $F/[\dot{x}(t)A_0]$ vs. $\dot{x}(t)$ ($t < t_{max}$, where t_{max} is the time for the second force peak) at different impact speeds were plotted, as shown in Fig. 3(b). Since $F/[\dot{x}(t)A_0]$ is proportional to μ [Eq. (1)], the plots in Fig. 3(b) reflect the relationship between μ and $\dot{x}(t)$ of the suspensions. As shown in Fig. 3(b), at a low strain rate, there is a peak due to the first peak in Fig. 3(a). At a higher strain rate, a second increase in $F/[\dot{x}(t)A_0]$ can be observed, after which $F/[\dot{x}(t)A_0]$ becomes almost constant, a behavior similar to that of a suspension under shear flow [2]. A key observation is that, although the curves in Fig. 3(b) were obtained from impact tests at different impact speeds (for which the force, displacement and speed as

functions of time are quite different from each other), the $F/[\dot{x}(t)A_0]$ vs. $\dot{x}(t)$ curves related to the solidification at higher strain rates essentially collapse into one curve. Because the first and second peaks are well separated for the impact test with an impact speed of 1.07 m s^{-1}, the starting $\dot{x}(t)$ for the solidification can be identified from the curve, and the value is approximately 100 s^{-1}. In squeezing flow, the squeezing strain rate is related to the shear rate $\dot{\gamma}$ by a factor of $\sqrt{3}$, and the corresponding starting $\dot{\gamma}$ for the shear thickening can be estimated to be approximately 170 s^{-1}, a value that agrees reasonably well with the result shown in Fig. 1. Consequently, the results of the 65.5 wt % suspension provide strong evidence that the impact-induced solidlike behavior is correlated with the shear thickening of the suspensions.

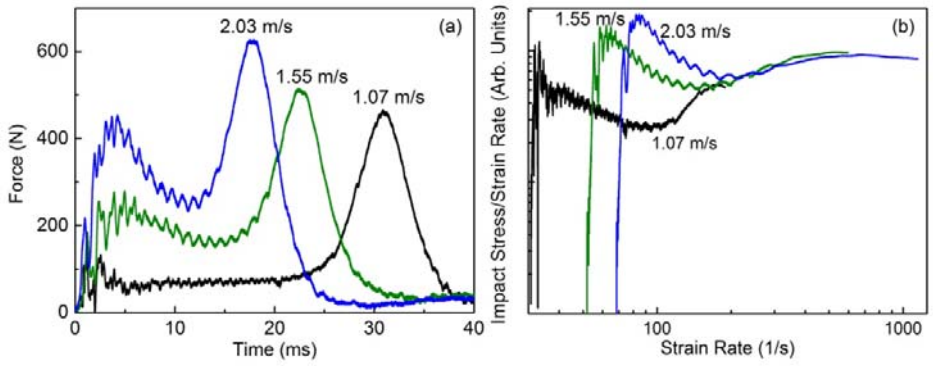

FIG. 3. (a) A summary of deceleration force vs. time curves under various impact speeds. (b) Impact stress/strain rate vs. strain rate curves of the 65.5 wt % silica suspension.

Impact tests with initial impact speeds of 1.03 m s^{-1} and 1.53 m s^{-1} were further performed on the 69 wt % (57.9 vol %) suspension. This suspension exhibits very

strong shear thickening, but its viscosity cannot be measured by a rheometer because of stress overloading. If tilted, slow flowing of the suspension in the container indicates that it is still in a fluidlike state. Because a higher impact speed could also overload the force sensor embedded in the impactor, the impact speed was limited to below 2.0 m s^{-1}. Figure 4 show the time dependence of the deceleration force, speed, and displacement of the impactor for the initial impact speeds of 1.03 m s^{-1} and 1.53 m s^{-1}, respectively. A strong deceleration force peak can be seen on each plot, reaching a value as high as 7000 N at the higher impact speed, which corresponds to a pressure of more than 2 MPa on the impactor.

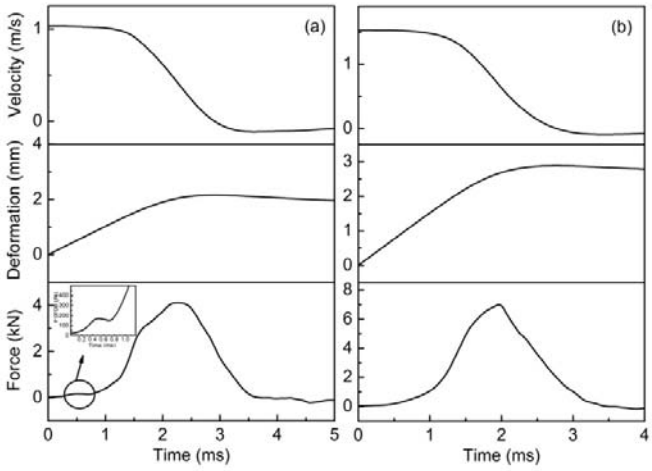

FIG. 4. Deceleration force, deformation of the suspensions (or displacement of the impactor) and impactor velocity vs. time for the 69 wt % silica suspension under initial impact speeds of (a) 1.03 m s^{-1}, and (b) 1.53 m s^{-1}. The inset in (a) shows a small force peak after the test starts.

As seen in supplemental movie 2, unlike the 65.5 wt % suspension, almost no flow of the 69 wt % suspension can be observed during the impact test [21]. Furthermore, a significant rebound of the impactor was observed, suggesting the

suspension exhibits significant elasticity under impact, an indication of impact induced solidlike behavior. Accordingly, in Fig. 4(a), less than 3 ms after the impact process was initiated, negative speed and reduction of displacement were observed, indicating the rebound of the impactor. The peak displacement was less than one tenth of the height of the suspension for both tests, which was close to the ratio of the average interparticle distance to the average distance between the centers of two particles in the suspension. The interparticle distance was estimated based on the following rationale. If the particle size is imagined to increase such that the particles are in contact (the interparticle distance is zero), we assume that the particles reach the maximum packing density (74 vol % for hard spheres). We can then estimate that the size of the particles with close packing is approximately 597 nm [$(0.74/0.589)^{1/3}$ times the particle size. Therefore, the interparticle distance at rest for a 69 wt % suspension is estimated to be approximately 50 nm. Since from movie 2, almost no fluidlike behavior can be observed, it is reasonable to deduce that the deformation of the suspension under impact is mainly caused by squeezing the solvent out between particles.

Similarly, $F/[\dot{x}(t)A_0]$ vs. $\dot{x}(t)$ [$t<t_{max}$, where t_{max} is the time for the intense force peak in Fig. 4 curves] for the 69 wt % suspension was plotted, as shown in Fig. 5(a). Unlike the 65.5 wt % suspension, the impact behavior of the 69 wt % suspension cannot be described by a single $F/[\dot{x}(t)A_0]$ vs. $\dot{x}(t)$ curve. For each impact speed, $F/[\dot{x}(t)A_0]$ first increases sharply with the initial increase in $\dot{x}(t)$ and then increases much more slowly as $\dot{x}(t)$ decreases. From Fig. 5(a), we can see

that the starting $\dot{x}(t)$ for the tests with initial speeds of 1.03 m s^{-1} and 1.53 m s^{-1} are approximately 50 s^{-1} and 70 s^{-1}, respectively, which must be well above the starting shear rate of shear thickening of the suspensions [Fig. 1(a)]. This implies that the suspension is directly transformed into a shear thickening state after the impact was initiated, which is consistent with the observation that almost no fluidlike behavior can be observed in the supplemental movie 2 [21]. Figure 5(a) also shows that the curves exhibit a similar trend, although a higher impact speed leads to a higher magnitude of $F/[\dot{x}(t)A_0]$ and a higher starting $\dot{x}(t)$. Some suspensions with a strong shear thickening have shown similar behavior when a shear stress ramp test was performed above a critical shear rate, as reported by Laun *et al*. [16]. The similarity of the results between the tests under shear and impact further suggests that the impact-induced solidlike behavior and shear thickening of the suspension are correlated.

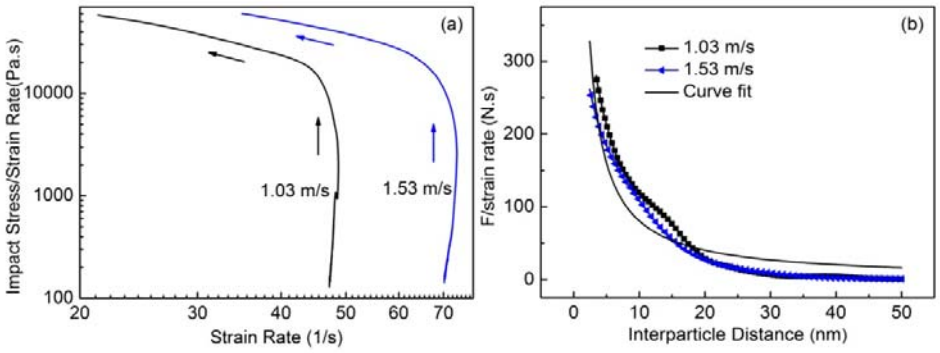

FIG. 5 (a) Impact stress/strain rate vs. strain rate curves of the 69 wt% silica suspension. The arrows indicate the change in the strain rate during the impact test. (b) Deceleration force/strain rate vs. interparticle distance curves for 69 wt % suspensions under different initial impact speeds. The figure also indicates that the experimental results can be approximately described by the function $y = b/x$ (the curve indicated by "Curve fit" in the figure).

B. Interparticle hydrodynamic force as the impact-induced solidification mechanism

Strong evidence has been provided for the correlation between impact-induced solidification and shear thickening in concentrated suspensions. Another question to be answered is the origin of the large impact-induced deceleration force and the associated significant energy dissipation. To resist the movement of the impactor, there must be some kind of resistive and/or repulsive force in the suspensions. Because the average interparticle distance in the suspensions is quite large (approximately 50 nm for the 69 wt % suspensions), the resistive or repulsive force should be relatively long range. One possibility is the electrostatic repulsive force. Because the silica/EG suspension is a nonaqueous colloidal suspension, the electrostatic repulsive force should be very weak and cannot be responsible for the large deceleration force on the impactor [27].

It was recently reported that frictional interaction between particles could play an important role in inducing shear thickening in concentrated suspensions [14]. However, because the particle size of the silica is smaller than 1 μm, the frictional force should not be effective in our study [28].

A possible resistive force causing the deceleration is the hydrodynamic force when the particles are pushed together, resulting in significant energy dissipation. Based on the hydrodynamic force, a simple model is proposed to explain the origin of

the deceleration force. At the beginning of the impact test, the concentrated suspension can be simplified into a line of nanoparticles of uniform interparticle distance, as shown in Fig. 6. If no boundary exists, the suspension will move with the impactor after the impact starts. With the boundary, the particle close to the boundary ("first particle") will be stopped (Fig. 6), resulting in a relative movement between this particle and its higher neighbor ("second particle"). The hydrodynamic lubrication force for the head-on collision of two particles can be expressed as

$$F_{hydro} = \left(3\pi\mu a^2 v_{rel}\right)/8\delta, \tag{3}$$

where v_{rel} is the relative velocity between two particles of diameter a and interparticle spacing δ [15]. For the 69 wt % suspension, in which the interparticle distance is less than one tenth of the particle diameter, Eq. (3) can be rewritten as

$$F_{hydro} \approx 3\pi\mu a^3 v_{rel}/[8(a+\delta)\delta], \tag{4}$$

When the impact test starts, the velocity of the first particle can be assumed to be zero, and the velocity of the second particle can be the same as the velocity of the impactor. Therefore, the v_{rel} between those two particles can be assumed to be equal to the velocity of the impactor. Because the suspension is predominantly solid with almost no flow during the impact, $v_{rel}/(a+\delta)$ is approximately equal to $l_0/(a+\delta)$ times the macroscopic strain rate $\dot{x}(t)$ (l_0 is the depth of the suspension). Therefore, the hydrodynamic lubrication force F_{hydro1} between the first set of two particles is proportional to $\dot{x}(t)/\delta$. The deceleration of the second particle could cause a relative movement between itself and its higher neighbor ("third particle") and result in a

hydrodynamic force between those particles. The transient v_{rel} between the two particles is proportional to the deceleration of the second particle, which is proportional to the hydrodynamic force F_{hydro1} between the first and second particles. Clearly, the hydrodynamic force F_{hydro2} between the second and third particles is proportional to F_{hydro1}. We can further deduce that the hydrodynamic force $F_{hydro(n-1)}$ between the nth and (n-1)th particles is also proportional to F_{hydro1}. It is reasonable to assume that the deceleration force F on the impactor is the sum of the hydrodynamic forces of a large number of particles close to the impactor. Consequently, F is proportional to F_{hydro1}, i.e., $F \propto F_{hydro1} \propto \dot{x}(t)/\delta$.

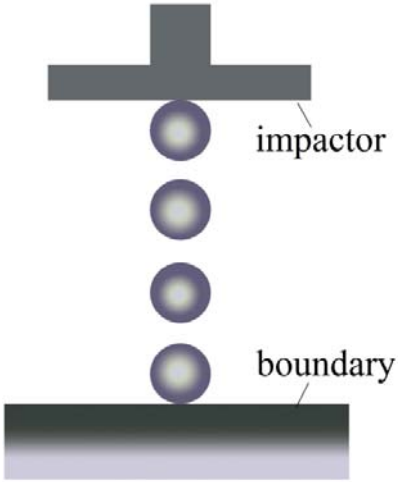

FIG. 6 Schematic illustration of the concentrated suspensions under impact. The suspension is represented by a line of particles (of exaggerated size), and the boundary is the bottom of the container.

Alternatively, the same conclusion can be reached based on the snowplow model [15]. F should be proportional to the hydrodynamic force F_{hydrof} of the particles at the solidification front. According to ref. [15], $v_{rel} \propto$ the velocity of the impactor. Therefore, F is also proportional to $\dot{x}(t)/\delta$ based on the snowplow model.

The $F/\dot{x}(t)$ vs. $\delta(t)$ curves of the 69 wt % suspension were plotted, as shown in Fig. 5(b). $\dot{x}(t)$ was directly calculated from the experimental results in Fig. 4, and

$$\delta(t) = 50 - 50D(t)/D_{max}, \tag{5}$$

where D_{max} is the maximum displacement from the experiments, which was estimated by assuming the interparticle distance at rest is 50 nm and is zero when D_{max} is measured.

As shown in Fig. 5(b), the two curves obtained from the impact tests with different initial impact speeds almost collapse into one curve. To further confirm that the large F originates from the hydrodynamic force, $F/\dot{x}(t)$ vs. $\delta(t)$ for the impact test with an initial speed of 1.53 m s^{-1} was fitted using the formula $y = b/x$, where b is a constant. As shown in Fig. 5(b), this function follows the trend of the experimental curves reasonably well. The deviation of the fitted curve from the experimental curves may be caused by the following factors. (a) δ is an estimation, and it may be affected by nonuniform particle sizes and the setting of maximum and zero interparticle distance. (b) Slight flowing of the suspension at the beginning of the impact test, manifested by a small force peak before the intense force peak shown in Fig. 4(a), and pushup of the suspension after the impact was initiated (supplemental movie 2) [21], may cause overestimation of $\dot{x}(t)$, which leads to a smaller experimental force than the fitted curve, especially at high δ. (c) At low δ, a short-range repulsive force from the surface layer of the SiO_2 particle may take effect,

which possibility we will discuss next.

With respect to the above discussion, it should be stressed that although nonuniform particle size and the setting of maximum and zero interparticle distance may affect the shape of the $F/\dot{x}(t)$ vs. $\delta(t)$ curves, the conclusion drawn from Fig. 5(b) will not be affected. When the interparticle distance at rest is estimated [Eq. (5)], we set the maximum concentration of the suspension to 74% (cubic-close-packing density). It could also be set to another concentration (for example, random-close-packing density), and the interparticle distance can be simply expressed as $50k$ nm, where k is a constant. Similarly, if the particle size is not monodispersed, we can use a representative average interparticle distance $50k_{aver}$ in the equation, where k_{aver} is a constant. This means that, if we use the same formula (Eq. (4)) to calculate $\delta(t)$, the two curves in Fig. 5(b) obtained at different impact speeds will collapse into one curve regardless of how we set the interparticle distance at rest. In this work, the polydispersity of the silica particles is small (< 10%) and is not a factor that has an important effect on our experimental results. When $\delta(t)$ is calculated, the interparticle distance is assumed to be zero at the end of the impact test, which is a reasonable simplification for manipulation of the data, although in reality the distance is not necessarily zero. The impact tests on the 69 wt % suspensions suggest the penetration of the impactor is close to 1/10 of the suspension depth. This means the interparticle distance is close to zero, or much smaller than the ~50 nm interparticle distance at the beginning of the impact test, and setting its value to zero does not significantly affect the discussion and conclusion related to Fig. 5(b).

Strong evidence has shown that the deceleration force on the impactor originates from the interparticle hydrodynamic force. Based on this simple hydrodynamic model, the magnitude of the deceleration force in the impact test of the 69 wt % suspension can be further estimated. The force experienced by the impactor should mainly come from the hydrodynamic force $F_{hydro(n-1)}$ of the particles just under the impactor (Fig. 6). We cannot derive an exact expression for $F_{hydro(n-1)}$, but because $F_{hydro(n-1)}$ is proportional to F_{hydro1}, as we discussed above, F_{hydro1} is used to estimate the order of the magnitude of the deceleration force F on the impactor. During the impact test, the number of the particles under the impactor can be estimated as

$$n = \pi[R/(a+\delta)]^2, \tag{6}$$

where R is the radius of the impactor (one inch). Therefore, the deceleration force F can be estimated as

$$F \approx F_{hydro1}\pi[R/(a+\delta)]^2, \tag{7}$$

Substituting Eq. (4) into Eq. (7), we obtain

$$F \approx 3\pi\mu\dot{x}(t)V/8\delta, \tag{8}$$

where V is the volume of the suspensions under the impactor, R=2.54 cm, μ=0.016 Pa.s, and l_0~30 mm. The exact strain rate and interparticle distance during the impact tests are not available, but from Fig. 5(a), if the initial impact speed is 1.03 m s^{-1}, the maximum strain rate is approximately 50 s^{-1}. We use this strain rate to estimate the order of magnitude of the deceleration force. If the interparticle distance is 50 nm, F can be estimated as approximately 1100 N and if the interparticle distance is 5 nm, F

is approximately 11000 N. The maximum impact force we observed is approximately 4000 N in Fig. 4(a). Consequently, based on the hydrodynamic force, the order of magnitude of the deceleration force measured on the impactor is consistent with the experimental results.

We propose that the large deceleration force on the impactor originates from the interparticle hydrodynamic force, but the possible effects of the relative movement between particles under impact on the concentration distribution of the suspension are not clear. A study has shown that the impact force is anisotropic, evidenced by the focused force transmission under impact, and it is possible that the particles become closer in the impact direction and further apart in the in-plane direction [5]. As a result, the suspension remains homogeneous, but not isotropic during the impact. On the other hand, a stress-induced variation in the concentration of concentrated suspensions has been proposed or observed in various studies [2,9,15,29]. It is therefore possible that under impact, the concentration of the suspension below the impactor increases due to the relative movement of the particles and accordingly, the concentration around the impactor could decrease. The rearrangement or movement of the particles in the suspension can be achieved by overcoming interparticle forces, such as the stochastic force for Brownian motion and hydrodynamic force [2]. Notably, these mechanism for particle rearrangement do not require overcoming Darcy pressure, as would be required if the suspension were simply treated as a porous medium. Indeed, it can be demonstrated that the Darcy flow would be negligible for this system, even under the maximum observed impact pressure (~2

MPa), since the permeability k_p, estimated using the Kozeny-Carman relation

$$k_p = \phi^3 a^2 / [180(1-\phi)^2], \quad (9)$$

where ϕ is the volume fraction of the suspension, and a is the particle size, is very small (of the order 10^{-14}-10^{-15} m^2) for a particle size of ~550 nm and a suspension volume fraction between 0.55 and 0.74 [30,31].

C. The elasticity of the suspension

Supplemental movie 2 shows that the 69 wt % suspension exhibits a significant rebound, which is one of the few pieces of evidence that directly demonstrates the ability of dense suspensions to store the energy elastically [21]. The hydrodynamic force can only dissipate the impact energy. Therefore, there must be a certain kind of repulsive force that can restore the suspension after impact. In our recent study, we provided strong evidence for the existence of a substantial amount of hydroxyl groups on the surface of silica particles [19,32]. A solvation layer, which is formed by adsorbing a polar solvent, such as EG, through hydrogen bonding with the hydroxyl groups, could be the source of repulsive interparticle interaction [19, 29,33-35]. We therefore postulate that the observed elasticity might be related to the solvation layer on the particle surface. Although in our study, the magnitude of the pressure and the effective distance across which the solvation layer can act is unknown, studies on water solvation layers have shown that solvation layers can produce very high pressures, up to 100 atm, and affect the particles at a distance of several nanometers [33-35]. During the impact tests, this short-range repulsive interaction could become

more effective at resisting the mutual approach of the particles in small δ, which may cause larger $F/\dot{x}(t)$ values than the fitted values shown in Fig. 5(b). At the end of the impact test, the elastic energy arising from this repulsive interaction may be released, causing significant rebound of the impactor.

Another possible mechanism for the rebound is elastic deformation of the particles when they are squeezed by the hydrodynamic force, or of the metal base on which the container sits, or of the plastic container [36]. However, an estimation of the stored energy due to the elastic deformation of the silica particles, metal base, or plastic container suggests that the contribution should be very minor if this mechanism is present. For the test with an initial impact speed of 1.03 m s^{-1} (Fig. 4(a)), a pressure of approximately 1.3 MPa on the impactor can be calculated. If we assume that the pressure is uniformly transferred to the silica particles in the suspensions, the pressure can cause a strain of approximately 0.2×10^{-4} (taking the elastic modulus as 70 GPa [37]). Therefore, the elastic energy stored per unit volume due to the elastic deformation (in the extreme case) can be estimated to be of the order of approximately 30 J m^{-3} (the product of the stress and strain). The volume of the silica in the suspension is approximately 100 cm^3, so the maximum elastic energy stored in the silica particles should be less than 3×10^{-3} J. From the impact video (supplemental material, movie 2) [21], we can see that the rebounding distance of the impactor is larger than 10 mm, which corresponds to an elastic energy of approximately 0.5 J (the product of the mass of the impactor, the g constant and the rebounding distance).

Similarly, the elastic energy from the plastic container or the metal base was

estimated, from which it is evident that this cannot be responsible for the observed rebound either. The container used in the impact test is made of polypropylene and has a wall thickness of ~1.6 mm. The elastic modulus of polypropylene is approximately 1.5-2 GPa. Therefore, under a pressure of 1.3 MPa, the elastic energy stored in the polypropylene can be estimated to be approximately 1.5×10^{-3}-2×10^{-3} J, much lower than the energy required for rebounding. The metal base is steel, and its elastic modulus is ~200 GPa. Under a pressure of 1.3 MPa, the strain is only ~6.5×10^{-6}. The elastic energy per volume is approximately 8.5 J m^{-3}. If the rebounding is caused by the elasticity of the metal, it requires the volume of the metal to be ~0.058 m^3. Since the impactor area is ~2×10^{-3} m^2, the height of the metal base would have to be approximately 30 m to generate 0.5 J elastic energy, which is not possible in our study.

Consequently, the rebound should mainly originate from the elasticity of the suspensions. This conclusion is further supported by the observation that when a bag of the concentrated silica/EG suspension on the ground was hit by a hammer, a significant rebound of the hammer was observed, but when the ground was hit directly with the hammer, no obvious rebound was observed.

D. Further remarks on the sample size

In this work, we provided strong evidence that impact induced solidlike behavior correlates with shear thickening behavior. Prior studies showing impact induced solidlike behavior of suspensions were performed on shear thickening fluids [5,6],

implying that the two phenomena may share a general mechanism. Similar to shear thickening, this work has shown that one controlling factor to induce solidlike behavior under impact is the strain rate, a parameter that is related to the size (depth) of the sample. In ref. [15], a large amount of cornstarch/water suspension was used with the intention of avoiding the effect of the size or boundary on the impact results. While the rheological properties of the specific cornstarch/water suspension used in that study are not known, cornstarch/water suspensions normally become shear thickening at a low shear rate (typically below 10 s^{-1}) [38], implying that, even with a large sample size, this boundary effect may be present. On the other hand, the silica/EG suspensions in the present work become shear thickening at a much higher shear rate (around or above 100 s^{-1}), and we can observe phenomena similar to those in ref. [15] using a smaller amount of the suspension. In the 65.5 wt % suspensions, we observed two force peaks, as also observed in ref. [15]. Another advantage of using a small sample size in the impact test is that the 69 wt % suspension can be directly converted into a true solid state upon impact, which provided us an opportunity to study the mechanisms of the observed deceleration force by minimizing the flow of the suspensions.

IV. CONCLUSIONS

Impact tests were performed on concentrated silica/ethylene glycol suspensions, and an impact induced solidlike behavior was observed. By analyzing the deceleration

force, velocity and displacement of the impactor, we provided strong evidence that impact induced solidlike behavior and shear thickening of the suspensions are correlated, and that the observed large deceleration force and significant energy dissipation during the impact test originate from the interparticle hydrodynamic force in the suspensions. Concentrated suspensions also exhibited impact induced elasticity, manifested by significant rebounding of the impactor. We propose that this elasticity originates from an interparticle repulsive force which arises from the solvation layer on the surface of the silica particles.

ACKNOWLEDGMENTS

The research, undertaken at the South Dakota School of Mines and Technology, was sponsored by the US Army Research Laboratory under Cooperative Agreement Number W911NF-08-2-0022, and the research at the University of Science and Technology of China was supported by the National Natural Science Foundation of China (No. 51373161), 1000 Young Talents Program, and Fundamental Research Funds for the Central Universities. We would like to thank Mr. Samuel French for his help on the impact tests.

References

[1] H. A. Barnes, J. Rheol. **33**, 329 (1989).

[2] N. J. Wagner and J. F. Brady, Phys. Today **62**, 27 (2009).

[3] R. J. Larsen, J. W. Kim, C. F. Zukoski, and D. A. Weitz, Phys. Rev. E **81**, 011502 (2010).

[4] M. I. Smith, R. Besseling, M. E. Cates, and V. Bertola, Nat. Commun. **1**, 114 (2010).

[5] B. Liu, M. Shelley, and J. Zhang, Phys. Rev. Lett. **105**, 188301 (2010).

[6] M. Roché, E. Myftiu, M. C. Johnston, P. Kim, and H. A. Stone, Phys. Rev. Lett. **110**, 148304 (2013).

[7] R. L. Hoffman, Trans. Soc. Rheol. **16**, 155 (1972).

[8] J. C. Van Der Verff and C. G. De Kruif, J. Rheol. **33**, 421 (1989).

[9] X. Cheng, J. H. McCoy, J. N. Israelachvili, and I. Cohen, Science **333**, 1276 (2011).

[10] M. E. Cates, M. D. Haw, and C. B. Holmes, J Phys. Condens. Matter **17**, S2517 (2005).

[11] B. J. Maranzano and N J Wagner, J. Rheol. **45**, 1205 (2001).

[12] S. Majumdar, R. Krishnaswamyb, and A. K. Sood, PNAS **108**, 8996 (2011).

[13] E. Brown, N. A. Forman, C. S. Orellana, H. J. Zhang, B. W. Maynor, D. E. Betts, J. M. DeSimone, and H. M. Jaeger, Nature Mater. **9**, 220 (2010).

[14] E. Brown and H. M. Jaeger, Rep. Prog. Phys. **77**, 046602 (2014).

[15] S. R. Waitukaitis and H. M. Jaeger, Nature **487**, 205 (2012).

[16] H. M. Laun, R. Bung, and F. Schmidt, J. Rheol. **35**, 999 (1991).

[17] Y. S. Lee, E. D. Wetzel, and N. J. Wagner, J. Mater. Sci. **38**, 2825 (2003).

[18] W. F. Jiang, X. L. Gong, S. H. Xuan, W. Q. Jiang, F. Ye, X. F. Li, and T. X. Liu Appl. Phys. Lett. **102**, 101901 (2013).

[19] B. J. Chu, A. T. Brady, B. D. Mannhalter, and D. R. Salem, J. Phys. D: Appl. Phys. **47**, 335302 (2014).

[20] E. Sevkat, B. Liaw, F. Delale, and B. B. Raju, Composites Part A **40**, 1090 (2009).

[21] See Supplemental Material for the movies of impact test of 65.5 wt % and 69 wt % suspensions

[22] J. W. Glasheen and T. A. McMahon, Phys. Fluids **8**, 2078 (1996).

[23] E. G. Richardson, Proc. Phys. Soc. **61**, 352 (1948).

[24] J. Engmann, C. Servais, and A. S. Burbidge, J. Non-Newtonian Fluid Mech. **132**, 1 (2005).

[25] S. Chatraei, C. W. Macosko, and H. H. Winter, J. Rheol. **25**, 433 (1981).

[26] B. Hoffner, C. Gerhards, and M. Peleg, Rheol. Acta **36**, 686 (1997).
[27] S. R. Raghavan, H. J. Walls, and S. A. Khan, Langmuir **16**, 7920 (2000).
[28] B. M. Guy, M. Hermes, and W. C. K. Poon, Phys. Rev. Lett. **115**, 088304 (2015)
[29] A. Fall, A. Lemaître, F. Bertrand, D. Bonn, and G. Ovarlez, Phys. Rev. Lett. **105**, 268303 (2010).
[30] P. Xu, and B. M. Yu, Adv. Water Resour. **31**, 74 (2008)
[31] R. Holdich, *Fundamentals of Particle Technology* (Midland Information Technology and Publishing, 2002)
[32] R. K. Iler, *The Chemistry of Silica* (John Wiley & Sons, New York, 1979).
[33] Y. Min, M. Akbulut, K. Kristiansen, Y. Golan, and J. N. Israelachvili, Nat. Mater. **7**, 527 (2008).
[34] J. N. Israelachvili and R. M. Pashley, Nature **306**, 249 (1983).
[35] H. Kamiya, M. Mitsui, H. Takano, and S. Miyazawa, J. Am. Ceram. Soc. **83**, 287 (2000).
[36] R. H. Davis, J. M. Serayssol, and E. J. Hinch, J. Fluid Mech. **163**, 479 (1986).
[37] W. Pabst and E. Gregorova, Ceramics-Silikáty **57**, 167 (2013).
[38] A. Fall, N. Huang, F. Bertrand, G. Ovarlez, and D. Bonn, Phys. Rev. Lett. **100**, 018301 (2008).

Figure Captions

FIG. 1. (a) Viscosity vs. shear rate curves for silica particle/ethylene glycol colloidal suspensions; (b) SEM image of silica particles.

FIG. 2. Deceleration force, deformation of the suspension (or displacement of the impactor), and impactor velocity vs. time for the 65.5 wt % silica suspension under initial impact speeds of (a) 1.07 m s^{-1}, (b) 1.55 m s^{-1}, and (c) 2.03 m s^{-1}.

FIG. 3. (a) A summary of deceleration force vs. time curves under various impact speeds. (b) Impact stress/strain rate vs. strain rate curves of the 65.5 wt % silica suspension.

FIG. 4. Deceleration force, deformation of the suspensions (or displacement of the impactor) and impactor velocity vs. time for the 69 wt % silica suspension under initial impact speeds of (a) 1.03 m s^{-1}, and (b) 1.53 m s^{-1}. The inset in (a) shows a small force peak after the test starts.

FIG. 5 (a) Impact stress/strain rate vs. strain rate curves of the 69 wt% silica suspension. The arrows indicate the change in the strain rate during the impact test. (b) Deceleration force/strain rate vs. interparticle distance curves for 69 wt % suspensions under different initial impact speeds. The figure also indicates that the experimental results can be approximately described by the function $y = b/x$ (the curve indicated by "Curve fit" in the figure).

FIG. 6 Schematic illustration of the concentrated suspensions under impact. The suspension is represented by a line of particles (of exaggerated size), and the boundary is the bottom of the container.